Acta Pharmaceutica Sinica B 2024;14(7):2977–2991

Chinese Pharmaceutical Association
Institute of Materia Medica, Chinese Academy of Medical Sciences

Acta Pharmaceutica Sinica B

www.elsevier.com/locate/apsb
www.sciencedirect.com

ORIGINAL ARTICLE

Disruption of cyclin D1 degradation leads to the development of mantle cell lymphoma

Ke Lu[a,b], Ming Zhang[c], Hongyu Qin[a,b,d], Siyu Shen[e], Haiqing Song[f], Hua Jiang[d], Chunxiang Zhang[g], Guozhi Xiao[h], Liping Tong[a], Qing Jiang[e], Di Chen[a,b,*]

[a]*Research Center for Computer-aided Drug Discovery, Shenzhen Institute of Advanced Technology, Chinese Academy of Sciences, Shenzhen 518055, China*
[b]*Faculty of Pharmaceutical Sciences, Shenzhen Institute of Advanced Technology, Shenzhen 518055, China*
[c]*Oncology Department, Johns Hopkins University School of Medicine, Baltimore, MD 21205, USA*
[d]*Division of Spine Surgery, the First Affiliated Hospital of Guangxi Medical University, Nanning 530021, China*
[e]*Division of Sports Medicine and Adult Reconstructive Surgery, Department of Orthopedic Surgery, Nanjing Drum Tower Hospital, Affiliated Hospital of Medical School, State Key Laboratory of Pharmaceutical Biotechnology, Nanjing University, Nanjing 210008, China*
[f]*Wenzhou Institute, University of Chinese Academy of Sciences, Wenzhou 325000, China*
[g]*Department of Cardiology, Basic Medicine Innovation Center for Cardiometabolic Diseases of Ministry of Education, Institute of Cardiovascular Research, the Affiliated Hospital, Southwest Medical University, Luzhou 646000, China*
[h]*School of Medicine, Southern University of Science and Technology, Shenzhen 518055, China*

Received 23 November 2023; received in revised form 12 January 2024; accepted 28 February 2024

KEY WORDS

Cyclin D1;
SUMOylation;
Mantle cell lymphoma;
Arsenic trioxide;
SENP2;
Proteasome degradation

Abstract Cyclin D1 has been recognized as an oncogene due to its abnormal upregulation in different types of cancers. Here, we demonstrated that cyclin D1 is SUMOylated, and we identified Itch as a specific E3 ligase recognizing SUMOylated cyclin D1 and mediating SUMO-induced ubiquitination and proteasome degradation of cyclin D1. We generated cyclin D1 mutant mice with mutations in the SUMOylation site, phosphorylation site, or both sites of cyclin D1, and found that double mutant mice developed a Mantle cell lymphoma (MCL)-like phenotype. We showed that arsenic trioxide (ATO) enhances cyclin D1 SUMOylation-mediated degradation through inhibition of cyclin D1 deSUMOylation enzymes, leading to MCL cell apoptosis. Treatment of severe combined immunodeficiency (SCID) mice

*Corresponding author.
E-mail address: di.chen@siat.ac.cn (Di Chen).

Peer review under the responsibility of Chinese Pharmaceutical Association and Institute of Materia Medica, Chinese Academy of Medical Sciences.

https://doi.org/10.1016/j.apsb.2024.03.013

grafted with MCL cells with ATO resulted in a significant reduction in tumor growth. In this study, we provide novel insights into the mechanisms of MCL tumor development and cyclin D1 regulation and discover a new strategy for MCL treatment.

1. Introduction

Cyclin D1 is the critical cyclin regulating the G1/S phase transition during normal cell cycle progression, and it forms a complex with CDK4/6 to act as a regulatory subunit in this process[1]. Multiple regulation processes exist to keep cyclin D1 expression under tight control during homeostasis, including proteosomal degradation[2,3]. Studies demonstrate that cyclin D1 is phosphorylated at T286, allowing it to be recognized by the ubiquitination degradation pathway, and that mutation of this site leads to its accumulation in the cell[4,5].

Cyclin D1 has been found to be upregulated in many different types of cancers, including breast cancer, mantle cell lymphoma (MCL), urinary bladder cancer, prostate cancer, non-small cell lung cancer, and colon cancer, etc.[6-13]. *CCND1*, the gene encoding for cyclin D1 protein, may function as a driver gene contributing to tumorigenesis. But exactly how cyclin D1 is dysregulated during cancer development is not known. Here, we determined the mechanism of this dysregulation and if this information could be useful for the cancer intervention.

Although Thr286 of cyclin D1 has been shown as the critical phosphorylation site responsible for the phosphorylation-mediated ubiquitin−proteasome degradation of cyclin D1[4,5], however, a later study demonstrated that the mutant cyclin D1 (T286A) could be still degraded by the ubiquitin−proteasome system[14], suggesting that the mechanism other than phosphorylation-mediated degradation may be involved in the cyclin D1 degradation. This finding makes us hypothesize that cyclin D1 protein may be regulated by another post-translational mechanism, such as SUMOylation-mediated ubiquitin-proteasome degradation.

In eukaryotic cells, SUMOylation functions as a three-step post-translational modification process similar to ubiquitination. The SUMO (small ubiquitin-like modifier) pathway regulates many aspects of normal protein function, such as their subcellular localization[15], the transactivation of transcription factors[16,17] and DNA repair[18]. Recent studies have reported that this modification mechanism is also involved in regulating cell cycle progression. For example, the SUMO-specific protease SENP5 is required for cell division[19]. In addition, Ubc9 (SUMO E2 enzyme) was found to regulate the activity of cyclins that are critical for S- and M-phase cell cycle progression[20]. In Xenopus oocytes with a Ubc9 loss-of-function mutant, several cell cycle proteins, such as CLB2/5, cyclin A, cyclin B, are stabilized[21].

Mammalian cells express three SUMO variants (SUMO1, SUMO2, and SUMO3)[22]. SUMO2 and SUMO3 proteins share 95% identity and are different from SUMO1 in their ability to form polymers. Because SUMO2 and SUMO3 cannot be distinguished by antisera, they are often referred to as SUMO2/3. SUMO1 shares ∼45% sequence identity with SUMO2 and is exclusively conjugated to target proteins as a monomer. SUMO is conjugated to lysine residues of protein substrates through an enzymatic process that requires a heterodimeric E1-activating enzyme, an E2-conjugating enzyme (UBC9), and one of the SUMO E3 ligases[23]. SUMOylation can be reversed by members of a family of proteases, called SENPs (sentrin- or SUMO-specific proteases)[24]. In this study we investigated if cyclin D1 is SUMOylated and deSUMOylated, as a means to regulate its protein levels.

Arsenic trioxide (ATO) has been approved for the treatment of acute promyelocytic leukemia[24]. ATO functions to disrupt the metabolic system of cells through allosteric inhibition of pyruvate dehydrogenase complex[25,26]. Several studies demonstrated that this compound induces cancer cell apoptosis, as well as cell cycle arrest at the G1 phase[27-29]. Further, several groups have found that ATO can target the fusion oncoprotein, PML-RARα. ATO directly binds with PML to induce a conformational change, leading to the SUMOylation of PML protein[30-32]. In this study, we examined if ATO could be used to inhibit MCL tumor growth.

Here, we discovered that cyclin D1 is SUMOylated, mediated by the SUMO-E3 ligase Itch, leading to its ubiquitination and proteasome degradation. We also mapped the SUMOylation site of cycle D1 protein. We then generated three strains of mice harboring cyclin D1 mutations at its phosphorylation site, its SUMOylation site or at both sites. We analyzed the phenotype of these mice and found that double mutant mice developed a MCL-like phenotype. We also showed that ATO enhances cyclin D1 SUMOylation, leading to its subsequent ubiquitination and proteasome degradation. We treated severe combined immunodeficiency (SCID) mice grafted with MCL cells with ATO and found that ATO inhibited tumor growth in these mice. We also found that ATO enhances cyclin D1 SUMOylation by inhibition of sentrin-specific protease (SENP) expression in MCL cells. Our findings have provided novel insights into cyclin D1 regulation during normal cell cycle progression and cancer development and identified new method and agent for MCL treatment.

2. Materials and methods

2.1. Mouse model

All animal experiments were carried out under protocols approved by Institutional Animal Care and Use Committee (IACUC) of Rush University Medical Center and all experimental methods and procedures were carried out in accordance with the approved guidelines to comply with all relevant ethical regulations for animal testing and research. T286A (B6J-Ccnd1em1Cin (T286A) Nju, T002526) mice, K149R (B6J-Ccnd1em1Cin (K149R) Nju, T002525) mice, DM (B6J-Ccnd1em1Cin (T286A & K149R) Nju, T002527) mice and NCG (NOD/ShiLtJGpt-Prkdcem26Il2rgem26/Gpt, T001475) mice were ordered from GemPharmatech. Genotyping was performed by PCR analysis of DNA isolated from mouse tails. The following genotyping primers were used:

T286A, forward primer 5′-TGCCAGGAACAGATTGAAGC-3′

T286A, reverse primer 5′-GCACGTCGGTGGGGGC-3′

K149R, forward primer 5′-ATCCGGGGGTACCGCGTCGAG-3′

K149R, reverse primer 5′-TTCTCTGTTTCCAGCCAACC-3′

DM, forward primer 5′-GGCCACCTCGCTACAGCAAC-3′

DM, reverse primer 5′-GGCCACCTCGCTACAGCAAC-3′

All animals were kept in a specific pathogen-free facility (SPF) in individually ventilated cages, 5 mice per cage, and the animals were in a 12-h day/night cycle and a controlled housing temperature at 22 °C. All animals were fed a standard chow diet (3.1 kcal/g; 2918 Teklad Global Protein rodent diet; Harlan). Most subjects from the study are the result of in-house mating and littermate controls were used. Male and female mice from 6 to 12 months of age were imported into the facility to complete experimental groups. The basic pathological phenotype and morbidity of mice were showed in Supporting Information Table S1.

For generating the xenograft model, each NCG mouse was inoculated subcutaneously in the flank with 5×10^6 Jeko-1 cells suspended in 50 μL of Basement Membrane Matrigel (Coring® Matrigel®) (Corning Life Sciences, Cat# 354234). Mice were weighed daily and watched for tumor formation. Once a tumor appeared, tumor width and length were measured at different time points. When the tumor size reached more than 1.0 cm^3, intratumoral ATO treatment (3.2 mg/kg) or Biotin-ATO[33] was initiated, with administration of the compounds performed 3 times per week. Tumor volumes were calculated by considering the average value of width and length of tumor as the radius of a sphere and using Eq. (1) for the volume of sphere:

$$V = 4/3\pi r^3 \quad (1)$$

Tumor weights were also measured after the mice were killed.

2.2. Cell culture

Human embryonic kidney 293 (293) cells were cultured in Dulbecco's modified Eagle's medium (DMEM) (Gibco, Cat# 11995040) supplemented with 10% fetal bovine serum (Gibco, Cat# 10100139C) at 37 °C under 5% CO_2. Human mantle cell lymphoma JeKo-1 cells were cultured in RPMI-1640 medium (Gibco, Cat# 61870143) supplemented with 20% fetal bovine serum at 37 °C under 5% CO_2. All the cell lines used in this study were ordered from ATCC (293, Cat# CRL-1573; JeKo-1, Cat# CRL-3006). All cell lines were tested for mycoplasma free before they were used.

2.3. Cell transfection

293, JeKo-1 cell lines expressing HA-cyclin D1 or HA-cyclin D1 (K149R, T286A, DM) were generated by transient transfection using Lipofectamine 3000. DNA plasmids were transiently transfected into cells in 6-cm culture dishes using Lipofectamine 3000 (Thermo Fisher, Cat# L3000008). Empty vector was used to keep the total amount of transfected DNA plasmid constant in each group in all experiments. Flag-EGFP plasmid was co-transfected as an internal control to evaluate transfection efficiency. Western blotting and immunoprecipitation (IP) assays were performed 24 h after transfection.

2.4. Protein extraction

The samples of tissues or cells were homogenized and incubated in RIPA Lysis and Extraction buffer (Thermo Fisher, Cat# 89901) supplemented with 1 mmol/L PMSF (Sigma−Aldrich, Cat# 10837091001), 1 m mol/L Na_3VO_4 (Sigma−Aldrich, Cat# 450243) and protease inhibitor cocktail (Thermo Fisher, Cat# 78410). Total proteins were collected by centrifugation at 4 °C for 15 min at 13,000×*g*. The sample buffer (4× Laemmli Sample Buffer, Bio-Rad, Cat# 1610747) was added and warmed at 99 °C for 5 min. Aliquot and store samples in the −80 °C refrigerator.

2.5. Western blot and immunoprecipitation

Western blotting and IP were performed as previously described[34]. The interaction between endogenous cyclin D1 and Itch was determined in 293 cells. Proteasome inhibitor MG132 (10 μmol/L) (Sigma−Aldrich, Cat# M7449) was added to the cell culture 6 h before cells were harvested for IP assay (Thermo Fisher, Cat# 26149). After separation, samples were electrotransferred onto a fit PVDF membrane and blocked with 4% non-fat milk for 1 h at room temperature. The primary antibody of cyclin D1 (1:20,000), cyclin D1 (T286) (1:1000), Myc (1:100), HA (1:100), β-actin (1:200), α-tubulin (1:200) was added and incubated at 4 °C for overnight. After washing with PBS-T (0.2% Tween 20), secondary antibodies (1:3000) were applied for 1 h at room temperature and washing with PBST again. Finally, incubating the blot in ECL Sensitivity substrate (Thermo Fisher, Cat# 34095) and expose the blot to imaging system. All the antibodies used in this paper are listed in Supporting Information Table S2.

2.6. SUMOylation and ubiquitylation assay

SUMOylated cyclin D1 or ubiquitylated cyclin D1 was detected by co-immunoprecipitation (co-IP) using anti-SUMO-2/3 antibody or anti-ubiquitin antibody conjugated beads, followed by immunoblotting with anti-cyclin D1 antibody or anti-HA antibody for cyclin D1 detection. For *in vitro* SUMOylation assay, HA-tagged cyclin D1 construct was transiently transfected into 293 cells. 48 h after the transfection, the cyclin D1 protein was purified using Pierce HA Tag IP/Co-IP Kit (Pierce, Cat# 26149). The purified cyclin D1 protein was incubated in the presence of ATP, SUMO2, SUMO E1 and SUMO E2 for 1 h (30 °C). SUMOylated cyclin D1 were detected using anti-SUMO-2/3 antibody.

2.7. In vitro protein decay assay

Cells were seeded in 15-cm culture dishes, and WT or mutant cyclin D1 (K149R, T286A, DM) construct was transiently transfected, respectively, into 293 cells. 24 h after transfection, cells were trypsinized and split into five 10-cm dishes. 12 h after recovery, cells were cultured in regular medium with 80 μg/mL cycloheximide (Sigma−Aldrich, Cat# 5087390001) for 0, 30, 60, 120, and 300 min before harvesting. Western blotting was performed to detect the decay of cyclin D1 proteins.

2.8. Plasmids and site-directed mutagenesis

Cyclin D1 (K149R), cyclin D1 (DM, K149R/T286A) and loss of function mutants of Itch (L112A, V530A, V730A, L112A/V530A/V730A) were generated using a site-directed mutagenesis

kit (Agilent, CS, USA, Cat# 200515). Other plasmids expressing HA-cyclin D1 and HA-cyclin D1 (T286A)[34], Itch[35] were purchased from Addgene as list below. All constructs were confirmed by sequencing.

pcDNA3-HA-Sumo1, Cat# 21154; pcDNA3 HA-Sumo2 WT, Cat# 48967; pcDNA3 MYC-Sumo3 WT, Cat# 48964; Flag-SENP1, Cat# 17357; 3xFLAG-SENP7, Cat# 42886; pcDNA cyclin D1 HA T286A, Cat# 11182; pcDNA cyclin D1 HA, Cat# 11181; pcDNA3/UBC9, Cat# 20082; Itch, Cat# 36197.

2.9. Cell cycle analysis

FACS analysis was performed as described in the research by[36]. For FACS analysis, HCT-116 cells were stably transfected with WT cyclin D1 or mutant cyclin D1 (K149R, T286A, DM). In some experiments, the cells were synchronized before the G1 phase through serum starvation for over 16 h or treated with ATO (2.5 μmol/L) for 16 h. The cells were then stained with propidim iodide (50 μg/mL) at 37 °C for 1 h. FACS samples were analyzed with a FACSCanto™ Flow Cytometry System (BD Biosciences). And the data were analyzed using FlowJo 7.6 software according to the manufacturer's instruction.

2.10. Cell proliferation assay

Anchorage-dependent cell proliferation was observed by crystal violet staining. Anchorage-independent cell proliferation was determined by a soft agar assay. Cells were seeded at a density of 2×10^3 cells per 35-mm cell culture dish in 0.35% agar and cultured for 14 days at 37 °C under 5% CO_2. Dishes were stained with 0.05% crystal violet. Colonies were counted in the entire dish, and the colony size was determined by a microcaliper.

2.11. Histology, immunohistochemistry and immunofluorescence

Spleen, liver, lymph node, gastro intestine and solid tumor tissue of sacrifice from WT or Mut mice, were fixed in 4% paraformaldehyde, dehydrated, and embedded in paraffin. 5-μm thick sections of tissue were cut and stained with hematoxylin and eosin (H&E). Typical MCL cell characteristics are determined by an experienced pathologist.

For IHC staining, rehydrated sections were heated at 95 °C in Antigen Unmasking Solution (Vector Laboratories, Cat# H-3301-250) for 10 min, and then sequentially treated with 3% H_2O_2, 0.5% Triton X-100, Avidin/Biotin Blocking Kit (Vector Laboratories, Cat# SP-2001). After blocking with 10% normal goat serum for 1 h, sections were treated with primary antibodies, including CyclinD1 (1:500), Ki67 (1:200), PCNA (1:100), Bcl2 (1:500), B220 (1:500), CD5 (1:200), CD19 (1:200), CD20 (1:200), CD3 (1:150), CD34 (1:200), Bcl6 (1:200), P53 (1:200) overnight at 4 °C and incubated with secondary biotinylated goat anti-rabbit or anti-mouse antibody for 30 min, followed by treatment with the VECTASTAIN Elite ABC Kit (Vector Laboratories, Cat# SP-2001). IHC signals were revealed by ImmPACT DAB Peroxidase Substrate (Vector Laboratories, Cat# SK-4105) and analyzed using ImageJ program.

For immunofluorescence (IF) assay, rehydrated sections were incubated with specific primary antibodies for biotin and Senp2, and then incubated with a peroxidase-conjugated anti-fluorescein antibody. For detection of fluorescent signal and VECTASHIELD Mounting Medium with DAPI (Vector Laboratories, Burlingame, CA, USA) was used to mount the slides. Images of histology, IHC and IF were captured using CellSens Imaging Software (Olympus) on an Olympus BX43 microscope, or a Zeiss LSM700 confocal microscope.

2.12. Flow cytometry

Flow cytometry analysis was performed as described in the research[37]. Cell suspensions from murine spleen, peripheral blood, bone marrow or lymph node were collected and then stained with antibodies specific for murine CD5 (Biolegend, Clone 53−7.3), CD19 (Biolegend, Clone 6D5), CD3 (Biolegend, Clone 17A2), CD23 (Biolegend, Clone B3B4). Flow cytometry was carried out on a BD LSRFortessa. Flow data were then analyzed using FlowJo software.

2.13. Cytotoxicity test

CCK-8 assay (Beyotime, China, Cat# C0038) was used to analyze the cytotoxicity of ATO on JeKo-1 cells according to the manufacturer's instructions. Briefly, JeKo-1 cells were transferred in 96-well plates at a density of 5×10^3/well. 2.5 μmmol/L ATO treated JeKo-1 cells at different time (1, 6, 24, 48 h). The standard protocol for assessing cell viability was then carried out.

2.14. TUNEL staining

Cell apoptosis was detected using fluorescent *in situ* terminal deoxynucleotidyl transferase-mediated uridine 5′-triphosphate-biotin nick end labeling (TUNEL staining). Sections were first permeabilized in 0.1% Triton X-100 in phosphate-buffered saline (PBS) for 8 min. TUNEL reaction mixture was obtained by adding terminal deoxynucleotidyl transferase to nucleotide mixture, as instructed by the manufacturer's manual (DeadEnd™ Fluorometric TUNEL System, Promega, Cat# G3250). Sections were counterstained nuclei with 4′-6-diamidino-2-phenylindole (DAPI).

2.15. Luciferase reporter assay

The plasmids of reporter constructs were co-transfected with 3XE2F-luc reporter construct and cyclin D1 expression plasmid into 293 cells. 24 h after transfection, the cell lysates were then collected, and luciferase activity was measured using a Promega Dual Luciferase reporter assay kit (Cat# E1910).

2.16. Synthesis of arsenic−biotin conjugates

In this work, Arsenic trioxide (Sigma−Aldrich, Cat# 311383) and Biotin (Sigma−Aldrich, Cat# B4501) were used to synthesize Biotin-As and Biotin-As-SS according to the literature[33,38].

2.17. Statistics

The sample size for each experiment was determined based on our previous experiences. All the data were expressed as mean ± SD, as indicated in the figure legends. Statistical analyses were completed with Prism GraphPad Prim 8.0 software. Unpaired Student's *t*-test (for two groups), one-way ANOVA (for multiple groups) and two-way ANOVA (for multiple groups) were used followed by the Tukey−Kramer test. $P < 0.05$ was considered significant and is denoted in the figures. Unless otherwise noted, all experiments were performed on 3 individual samples. All the

mice were randomly assigned to different groups and the experiments were done in a blinded fashion.

3. Results

3.1. Cyclin D1 is sumoylated

To determine if cyclin D1 is SUMOylated, we transfected 293 cells with cyclin D1 and with SUMO1, SUMO2, SUMO3 or Ubc9 (the SUMO E2 enzyme). We found that all of these SUMO E2 or E3 enzymes induce cyclin D1 degradation (Fig. 1A–D and Supporting Information Fig. S1A–S1D). SUMO- or Ubc9-induced cyclin D1 degradation can be reversed by expression of the deSUMOylation enzyme SENP1 or proteasome inhibitor MG132 (Fig. 1A–D and Fig. S1A–S1D). These findings suggest that cyclin D1 is SUMOylated and subsequently degraded by the ubiquitin-proteasome system.

We then performed a cyclin D1 SUMOylation assay by co-transfection of HA-cyclin D1 with Ubc9 or SENP1 plasmid in the presence of MG132 in 293 cells. SUMOylated proteins were immunoprecipitated by the anti-SUMO2/3 antibody and SUMOylated cyclin D1 was detected by Western blot using the anti-HA antibody. We found that cyclin D1 was markedly SUMOylated and expression of SENP1 completely blocked the cyclin D1 SUMOylation (Fig. 1E). To determine the SUMOylation site of cyclin D1, we performed bioinformatics analysis and identified several putative SUMOylation sites. We then made a series of point mutation constructs of cyclin D1 and co-transfected WT or mutant cyclin D1 with Ubc9. We found that Ubc9 could not induce the degradation of cyclin D1 when the lysine 149 (K149) is mutated (Fig. S1E–S1G). We further determined the importance of K149 in cyclin D1 SUMOylation by transfection of HA-tagged WT or mutant cyclin D1 (K149R) with SUMO2 into 293 cells. SUMOylated proteins were pulled down by a SUMO2 antibody and SUMOylated cyclin D1 was detected by Western blot using an anti-HA antibody. We detected SUMOylation of WT cyclin D1, but not K149R mutant cyclin D1 (Fig. 1F). Phosphorylation-induced cyclin D1 degradation is found to occur mainly during S phase[5]. This finding was consistent with our observation that phospho-cyclin D1 levels increased dramatically at the 12 h time point (Fig. S1H–S1I). We also performed a pulse-chase assay to determine the protein stability of WT and mutant cyclin D1 and found that the cyclin D1 degradation was prolonged by either mutation at the phosphorylation site (T286A) or mutation at the SUMOylation site (K149R) of cyclin D1 (Fig. 1G–H). It seems that SUMOylation-induced cyclin D1 degradation is independent from the phosphorylation-induced cyclin D1 degradation, as mutation of both the phosphorylation site and the SUMOylation site make cyclin D1 even further stable then either mutation alone (Fig. 1G–H). Indeed, the K149R/T286A double mutant (DM) cyclin D1 was not degraded even 12 h after cycloheximide treatment (Fig. 1I and J). We then compared the degradation of mutant cyclin D1 with WT cyclin D1 and found that both Ubc9 and DDB2 (F-box E3 ligase) induced WT cyclin D1 degradation, whereas DDB2, but not Ubc9, induced K149R mutant cyclin D1 degradation and Ubc9, but not DDB2, induced T286A mutant cyclin D1 degradation, while both Ubc9 and DDB2 lost their ability to induce cyclin D1 degradation in the DM cyclin D1 (Fig. 1K). To determine if mutant cyclin D1 could also activate the downstream transcription factor E2F, which is one of the major functions of cyclin D1, we performed an E2F luciferase assay and found that E2F reporter activity was significantly increased in 293 cells transfected with WT or mutant cyclin D1 constructs, with the DM cyclin D1 showing the greatest activity (Fig. 1L). These findings indicate that mutations of cyclin D1 lead to cyclin D1 protein more stable with higher functional activity.

3.2. The SUMO E3 ligase Itch induces cyclin D1 SUMOylation

It has been reported that cyclin D1 interacts with Hect-domain E3 ligase Itch[40] and bioinformatics analysis showed that Itch contains 7 putative SUMO-interacting motifs. To determine if Itch induces cyclin D1 degradation, we co-transfected Itch with WT or mutant cyclin D1 and found that Itch induced degradation of WT and T286 mutant cyclin D1, but not K149R mutant cyclin D1 (Fig. 2A). Transfection of Itch into 293 cells induced endogenous cyclin D1 degradation (Fig. 2B). Co-transfection of SUMO or Ubc9 siRNA with Itch reversed Itch-induced cyclin D1 degradation (Fig. 2B and C). We then determined the effect of Itch on cyclin D1 ubiquitination by co-transfection of Itch with WT or mutant cyclin D1. We found that Itch induced the ubiquitination of WT and T286A mutant cyclin D1, but not K149R mutant cyclin D1 (Fig. 2D). We then identified the SUMO-interacting motifs of Itch by co-transfection of cyclin D1 with WT or mutant Itch with mutations of SUMO-interacting motifs. We found that Itch protein with mutations in either L112A, V530A, or V730A almost completely abrogated Itch binding to cyclin D1, and that the triple mutant showed complete loss of binding (Fig. 2E and F) and these binding patterns were consistent with the cyclin D1 degradation pattern. Single mutation of Itch led to reduce its activity to induce cyclin D1 degradation and triple mutations of Itch caused completely lost of its activity to induce cyclin D1 degradation (Fig. 2G). We then analyzed endogenous cyclin D1 levels in different organs in WT and *Itch* KO mice and found that cyclin D1 protein levels were significantly elevated in colon, spleen, stomach, and bone tissues of *Itch* KO mice (Fig. 2H).

3.3. Cyclin D1 DM mice display a mantel cell lymphoma-like phenotype

To determine whether inhibition of cyclin D1 degradation leads to specific type of cancer, we generated mice with various cyclin D1 mutations, including mutations of the SUMOylation site at K149, the phosphorylation site at T286, or both sites (refer to DM mice). We found that 12-month-old cyclin D1 DM mice showed a tumor-like phenotype in the abdomen or lateral canthus. We then screened different organs in the entire body of the three different cyclin D1 mutant mice and found that the spleen and the lymph nodes were affected in the K149R/T286A DM mice (Fig. 3A and B and Supporting Information Fig. S2A and S2B). The sizes of the spleens and the lymph nodes were significantly enlarged in the cyclin D1 DM mice (Fig. 3C and D). In addition, we also observed a tumor metastasis phenotype (Fig. S2C). To further confirm the tumor features in the DM mice, we performed histological analysis and found that the tumor cells have an MCL-like phenotype in the spleen, the lymph nodes, the liver and the tumor tissues of 6-month-old and 12-month-old DM mice (Fig. 3E–G and Fig. S2D–S2G).

We next performed immunohistochemistry (IHC) analysis in the spleen tissue of 6- and 12-month-old WT and cyclin D1 DM mice using antibodies against different cell surface markers, and we quantified the IHC data from the 12-month-old mice. We found

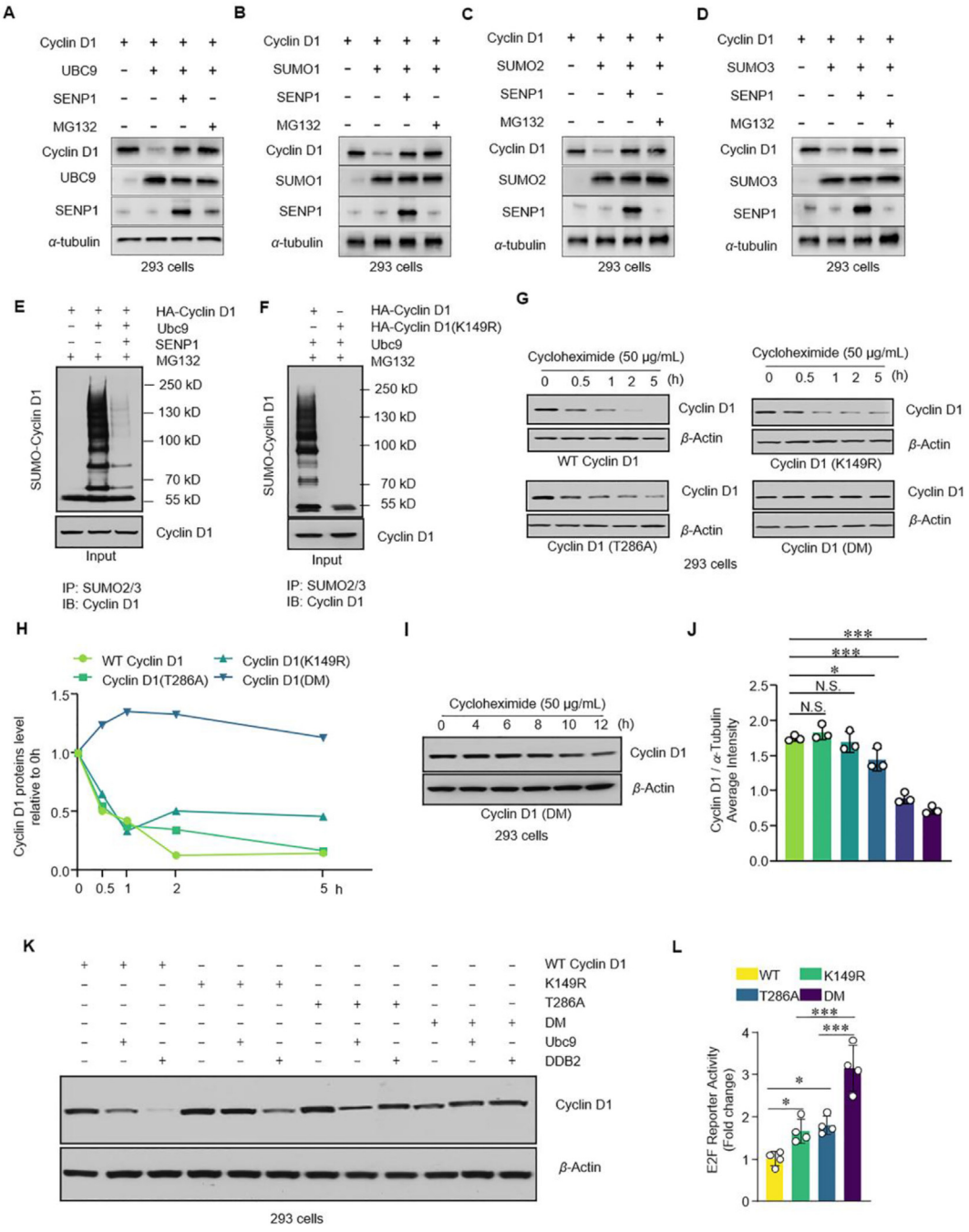

Figure 1 Cyclin D1 is SUMOylated leading to its proteasomal degradation. (A−D) Cyclin D1 expression in 293 cells co-transfected with Ubc9 (A), SUMO1 (B), SUMO2 (C), SUMO3 (D) plasmids with or without SENP1 plasmid or in the absence or presence of proteasome inhibitor MG132. (E) Immunoprecipitation (IP) assay showing SUMOylation and ubiquitination of cyclin D1 in 293 cells co-transfected with HA-cyclin D1 and Ubc9 or Ubc9+SENP1 plasmids in the presence of MG132. IP was performed using the anti-SUMO2/3 antibody (upper panel) or anti-Ub anti-body (lower panel) using the anti-HA antibody. Cyclin D1 expression in cell lysates was used as an input control. (F) IP assay showing cyclin D1 SUMOylation in 293 cells transfected with HA-cyclin D1 or mutant HA-cyclin D1 (K149R) plasmid. IP was performed using the anti-SUMO2 antibody followed by a Western blot using the anti-HA antibody. Cyclin D1 expression in cell lysates was detected as an input control. (G and H) Pulse-chase assay showing changes in cyclin D1 stability in 293 cells transfected with WT or mutant cyclin D1 [K149R, T286A and K149R/T286A double mutant (DM)] plasmids and treated with cycloheximide for 6 h. Cyclin D1 expression was detected at different time points after cycloheximide treatment (G). Quantification of cyclin D1 proteins level relative to 0 h (H). (I and J) Cyclin D1 expression in 293 cells transfected with WT or mutant cyclin D1 (DM) expression plasmid and treated with cycloheximide (CHX). Cyclin D1 expression was detected at different time points after CHX treatment (I). The Average Intensity of cyclin D1 relative to β-actin (J) ($n = 3$). (K) Cyclin D1 expression in 293 cells co-transfected with WT or mutant cyclin D1 (K149R, T286A or double mutant) and Ubc9 or DDB2 plasmids. (L) E2F-Luc reporter activity as determined by dual luciferase assay in 293 cells transfected with E2F-Luc reporter construct and WT or mutant cyclin D1 (K149R, T286A and DM) plasmids ($n=4$). $^{*}P < 0.05$, $^{**}P < 0.01$, $^{***}P < 0.001$. Data are represented as mean ± SD. One-way ANOVA followed by Tukey−Kramer test for multiple comparisons (J and L).

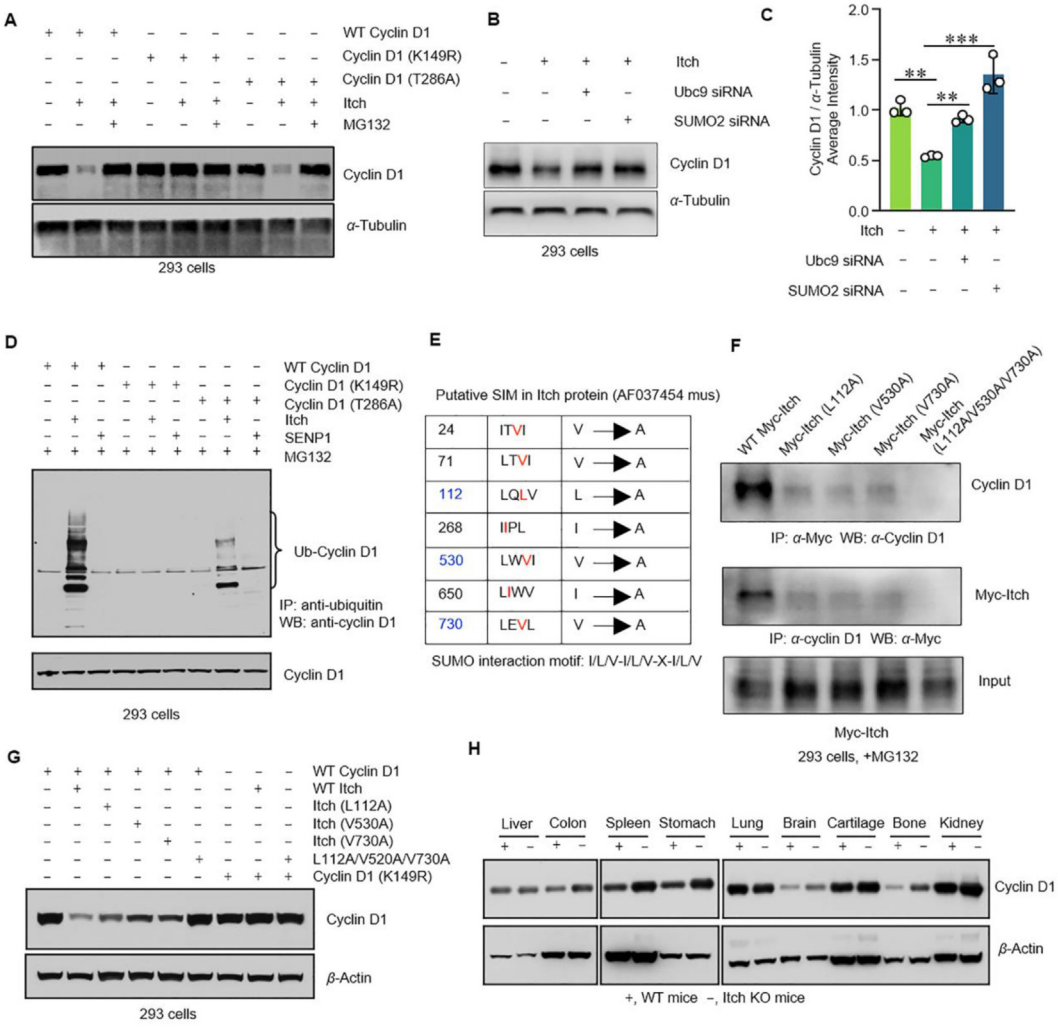

Figure 2 SUMO E3 ligase Itch induces cyclin D1 SUMOylation. (A) Cyclin D1 expression in 293 cells transfected with WT or mutant cyclin D1 (T286A and K149R mutants) and Itch plasmids in the absence or presence of the proteasome inhibitor MG132 (10 μmol/L, 6 h of incubation). (B and C) Cyclin D1 expression in 293 cells transfected with Itch and SUMO2 or Ubc9 siRNA (B). The Average Intensity of cyclin D1 relative to α-tubulin (C) ($n = 3$). (D) IP assay showing cyclin D1 ubiquitination in 293 cells co-transfected with WT or mutant cyclin D1 (T286A and K149R mutants) plasmids and Itch or SENP1 plasmid in the absence or presence of the proteasome inhibitor MG132. IP was performed using the anti-Ub antibody followed by the Western blot using the anti-cyclin D1 antibody. Cyclin D1 expression in cell lysates was detected as an input control. (E) Bioinformatics analysis of SUMO interaction motifs (SIMs) of Itch protein and generation of mutant Itch constructs. (F) IP assay showing cyclin D1 interaction with WT or mutant Myc-Itch with mutations in a single SIM (112, 530 and 730) or with a triple mutation in the presence of MG132 in 293 cells. IP was performed using either the anti-Myc antibody or the anti-cyclin D1 antibody followed by the Western blot using the anti-cyclin D1 or the anti-Myc antibody. Myc-Itch expression in cell lysates was detected as an input control. (G) Cyclin D1 expression 293 cells transfected with WT or mutant cyclin D1 (K149R) with WT or mutant Itch plasmids with a single SIM mutation (112, 530 and 730) or with a triple mutation. (H) Western blot analysis showing cyclin D1 expression in different tissues derived from WT or Itch KO mice. $^{*}P < 0.05$, $^{**}P < 0.01$, $^{***}P < 0.001$. Data are represented as mean ± SD, $n = 3$. Two-way ANOVA followed by Tukey−Kramer test for multiple comparisons (C).

that the numbers of cyclin D1-, B220-, CD5-, CD19-, Ki67-and Bcl2-positive staining cells were significantly greater in spleen cells of cyclin D1 DM mice compared to WT mice (Fig. 3H and Supporting Information Fig. S3A−S3F). In addition, expression of cyclin D1 was also significantly higher in the spleen cells of cyclin D1 K149R mutant and T286A mutant mice compared to WT mice (Fig. 3H and Fig. S3A). CD5-and PCNA-positive staining cells were also significantly greater in the spleen tissues of cyclin D1 K149R mutant mice compared to WT mice (Fig. 3H and Fig. S3D and S3H). We found that the numbers of PCNA- and CD20-positive staining cells were also significantly greater in the spleen tissues of cyclin D1 DM mice compared to WT mice (Fig. S3G−S3I). In contrast, no significant changes were found in the numbers of CD3-, CD34-, Bcl6-and P53-positive staining cells in the spleen tissues of DM mice compared to WT mice (Fig. S3G, S3J−S3M). These findings are consistent with the features of Mantle cell lymphoma, which is typically marked by overexpression of cyclin D1 in association with a chromosomal translocation.

We also analyzed the lymphoma phenotype in liver and intestine tissues of WT and DM mice and found that Ki67-and PCNA-

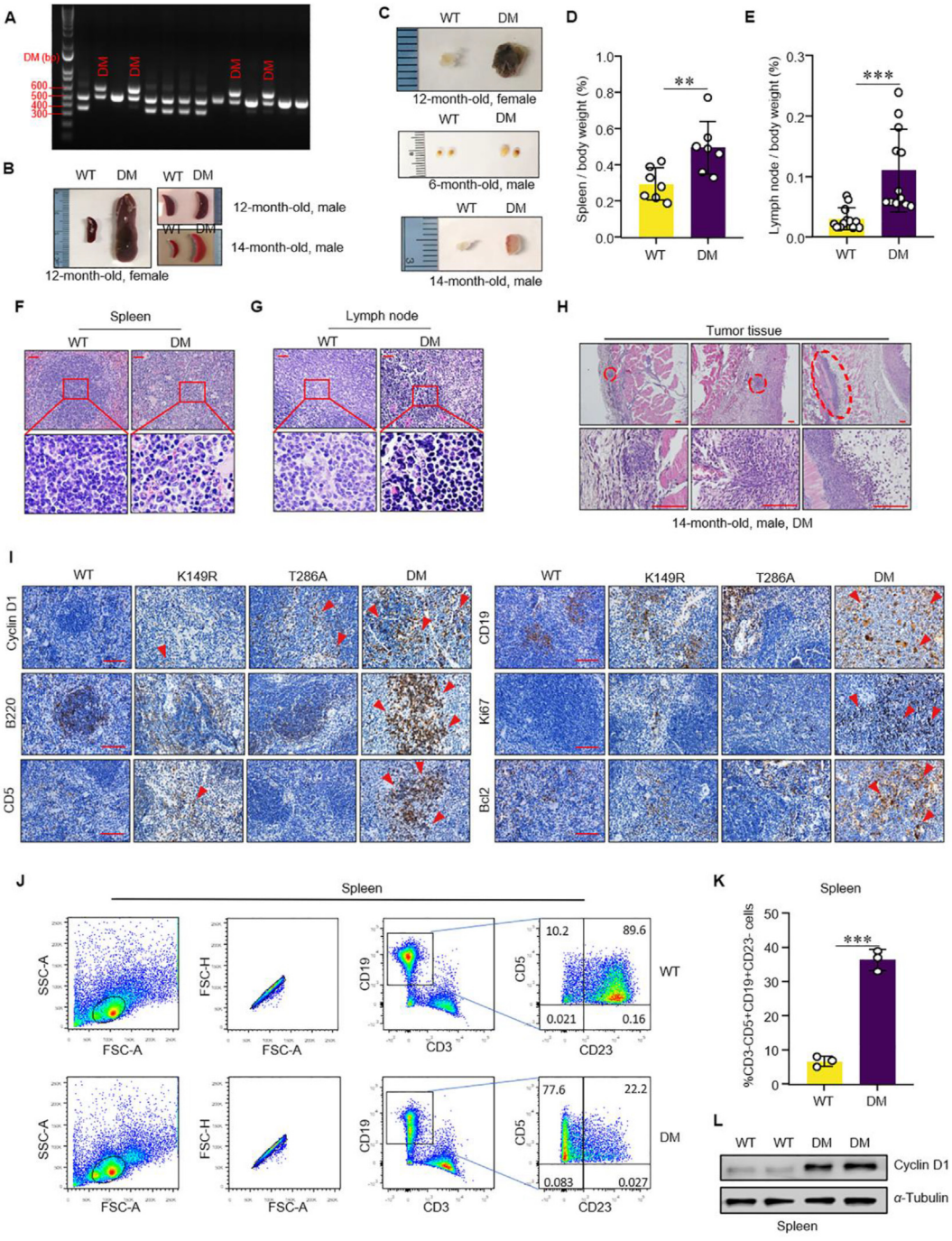

Figure 3 Characterization of the MCL-phenotype of cyclin D1 DM mice. (A) Representative genotyping data of cyclin D1 DM mice, 496 bp for WT; 355 bp for non-flpped; >500 bp (about 600 bp from previous results) for flpped. (B−E) Representative images showing gross anatomy of the spleen (B) and lymph node (C) in WT or mutant cyclin D1 [K149R, T286A and K149R/T286A double mutant (DM)] knockin mice. The ratio of spleen weight/body weight (D) ($n=7$) and the ratio of lymph node weight/body weight (E) ($n=12$) were calculated in WT and DM mice. (F−H) Representative H&E images showing histological changes in spleen (F), lymph node (G) of DM mice ($n=6$) (Scale bars, 25 μm), compared with those of WT mice and tumor tissue (H) in DM mice ($n=3$) (Scale bars, 75 μm). (I) Representative IHC images showing cell number changes in cyclin D1$^+$, B220$^+$, CD5$^+$, CD19$^+$, Ki67$^+$ and Bcl2$^+$ cells in spleen of K149R, T286A and DM mice and compared to those of WT mice (Scale bars, 50 μm) ($n=9$). (J and K) Flow cytometry images (J) and quantification (K) of CD3$^-$/CD5$^+$/CD19$^+$/CD23$^-$ cells in spleens of WT and DM mice ($n=3$). (L) Cyclin D1 expression in spleen tissues of WT and DM mice. *$P < 0.05$, **$P < 0.01$, ***$P < 0.001$. Data are represented as mean ± SD. Two-tailed unpaired Student's t-test analysis (D, E and K).

positive staining cells were significantly greater in the cyclin D1 DM mice (Supporting Information Figs. S4A–S4D, S5A–S5D). In addition, expression of Bcl2, B220, CD5, CD19, CD20 and P53 was also significantly greater in liver and intestine tissues of cyclin D1 DM mice compared to WT mice (Figs. S4E–S4I, S4M and S5E–S5I, S5M). In contrast, no significant changes were found in the numbers of CD3-, CD34-and Bcl6-positive staining cells in the liver and intestine tissues of cyclin D1 DM mice compared to WT mice (Figs. S4E–S4L, S5E–S5L). These phenotypic changes are consistent with the results observed in the spleen cells.

Cyclin D1 DM mice also formed solid tumors and liver metastasis (Fig. 3G and Fig. S2C and S2G). After analyzing the solid tumors by IHC, we found high levels of cyclin D1 expression in tumor tissues compared with that in adjacent tissues (Supporting Information Fig. S6A). We detected large amounts of Ki67-and PCNA-positive staining cells in the tumor tissues compared with that in adjacent tissues (Fig. S6B and S6C). Tumor tissues also expressed high levels of Bcl2, B220, CD3, CD5, CD31 and P53 (Fig. S6D–S6J). In contrast, no significant changes in CD34 expression were seen between the tumor tissues and adjacent tissues of cyclin D1 DM mice (Fig. S6K). There was a slight increase in Bcl6 expression in cyclin D1 DM mice compared with that in adjacent tissues (Fig. S6L). These findings are consistent with the results observed in the spleen, liver and intestine tissues.

We then performed flow cytometry assay using the cells isolated from the spleens, lymph nodes, bone marrow and blood cells of WT and cyclin D1 DM mice. We found that the percentage of $CD3^-/CD5^+/CD19^+/CD23^-$ cells were significantly greater in all these samples in 6-month-old cyclin D1 DM mice compared to WT mice (Fig. 3I and J and Supporting Information Fig. S7A–S7F). We also performed Western blot analysis using cell lysates isolated from WT and cyclin D1 DM mice and found that cyclin D1 expression was greater in cyclin D1 DM mice compared to WT mice (Fig. 3K and Fig. S7G–S7H). These findings are consistent with the results of IHC data.

3.4. *Arsenic trioxide enhances cyclin D1 sumoylation and degradation*

Arsenic trioxide (ATO) has been showed to enhance PML protein SUMOylation and degradation in acute myeloid leukemia (AML) cells[39]. To determine the effect of ATO on cyclin D1 SUMOylation, we performed SUMOylation and ubiquitination assays and found that ATO (2.5 μmol/L) enhanced cyclin D1 SUMOylation and ubiquitination in 293 cells as rapidly as 1 h after ATO treatment and addition of MG132 inhibited cyclin D1 SUMOylation and ubiquitination in 293 cells (Fig. 4A). We transfected WT and mutant cyclin D1 expression plasmids into 293 cells and treated cells with ATO (2.5 μmol/L) and found that ATO enhanced cyclin D1 SUMOylation and ubiquitination in the cells transfected with WT or T286A mutant cyclin D1 constructs, but not in the cells transfected with K149R mutant cyclin D1 construct in 293 cells (Fig. 4B). We also found that SUMOylation was enhanced in JeKo-1 cells treated with ATO (2.5 μmol/L; 0.5, 1 and 2 h) (Fig. 4C). The levels of SUMOylated cyclin D1 and polyubiquitinated cyclin D1 were significantly increased in JeKo-1 cells (a MCL cell line) with ATO treatment (2.5 μmol/L, 2 h) (Fig. 4D and E). Consistent with these findings, ATO-induced cyclin D1 inhibition could be reversed by SUMO1, SUMO2, SUMO3, Ubc9, or Itch siRNAs (Fig. 4F–J, Supporting Information Fig. S8A). In JeKo-1 cells, transfection of Ubc9 induced cyclin D1 degradation, which was reversed by SENP1, SENP2, SENP3, or SENP5 (Fig. S8B). SENP6 and SENP7 had only weak effects on reversing Ubc9-induced cyclin D1 degradation (Fig. S8B). Consistent with the ATO effect in 293 cells, ATO also enhanced WT cyclin D1 degradation in JeKo-1 cells compared to PBS-treated control cells (Fig. 4K–I), and cyclin D1 DM showed greater stability in JeKo-1 cells upon ATO treatment compared to the endogenous WT cyclin D1 (Fig. S8C).

3.5. *Arsenic trioxide inhibits tumor growth in scid mice grafted with MCL cells*

To determine if ATO could be used as a potential drug for MCL treatment, we examined the effect of ATO on cell death and cell viability in JeKo-1 cells. We found that treatment with ATO caused dose- and time-dependent cell death in JeKo-1 cells (Fig. 5A). The cell viability was also lower in JeKo-1 cells treated with ATO compared to the control cells (Fig. 5B). We also treated JeKo-1 cells with ATO and performed flow cytometry assay. We found that treatment with ATO resulted in significantly greater cells apoptosis in WT cells (Fig. 5C). In contrast, ATO had no significant effect on JeKo-1 cell apoptosis when the cells were transfected with cyclin D1 DM plasmid (Fig. 5C). To further determine the effect of ATO on MCL tumor growth *in vivo*, Jeko-1 cells suspended in 50 μL of Basement Membrane Matrigel were inoculated subcutaneously into NCG-SCID mice. When the tumor size reached to 1.0 cm^3, we initiated intratumoral ATO treatment (3.2 mg/kg), 3 times per week for 2 weeks. We found that the tumor volume and tumor weight were significantly lower in the ATO treatment group (Fig. 5D–F). We then performed IHC analysis on tumor tissues from control (Ctrl) mice or ATO-treated mice. We found that expression levels of cyclin D1, Ki67, BCL2, B220 (Fig. 5G–N), as well as CD5 and CD19 (Supporting Information Fig. S9) were significantly reduced in tumor tissues treated with ATO. We also performed flow cytometry assay using the cells isolated from the blood of Ctrl mice or ATO-treated mice. We found that the percentage of $CD3^-/CD5^+/CD19^+/CD23^-$ cells were significantly lower in the blood with ATO treatment (Fig. 5O and P).

3.6. *Arsenic trioxide may change SENP2 levels in DM mice*

SENP2 was reported to deconjugate SUMO1, SUMO2 and SUMO3 from targeted proteins, by cleaving an epsilon-linked peptide bond between the C-terminal glycine of the mature SUMO and the lysine epsilon-amino group of the target protein[40]. To evaluate if SENP2 was involved in the SUMOylation process in MCL cells, we examined the expression of SENP2 in DM mice and found SENP2 was significantly upregulated in the spleen, lymph nodes, intestine and liver tissues compared with that in WT mice (Fig. 6A–E). To determine if ATO enhances cyclin D1 SUMOylation through inhibition of SENP2, we labeled ATO with Biotin according to the procedure described previously (Supporting Information Fig. S10)[33]. We detected SENP2 binding to the Arsenic by co-IP assay in which the Arsenic binding proteins were immunoprecipitated by the anti-Biotin antibody and the SENP2, which interacts with Arsenic–Biotin, was detected by Western blot using the anti-SENP2 antibody (Fig. 6F). We further demonstrated that ATO-enhanced cyclin D1 degradation can be reversed by SENP2, but not SENP7 (Fig. 6G and H). In JeKo-1 cells, SENP2 was significantly decreased with ATO treatment (Fig. 6I and J). Taken together, SENP2 plays key role in deSUMOylation of cyclin D1 to maintain high level of cyclin D1

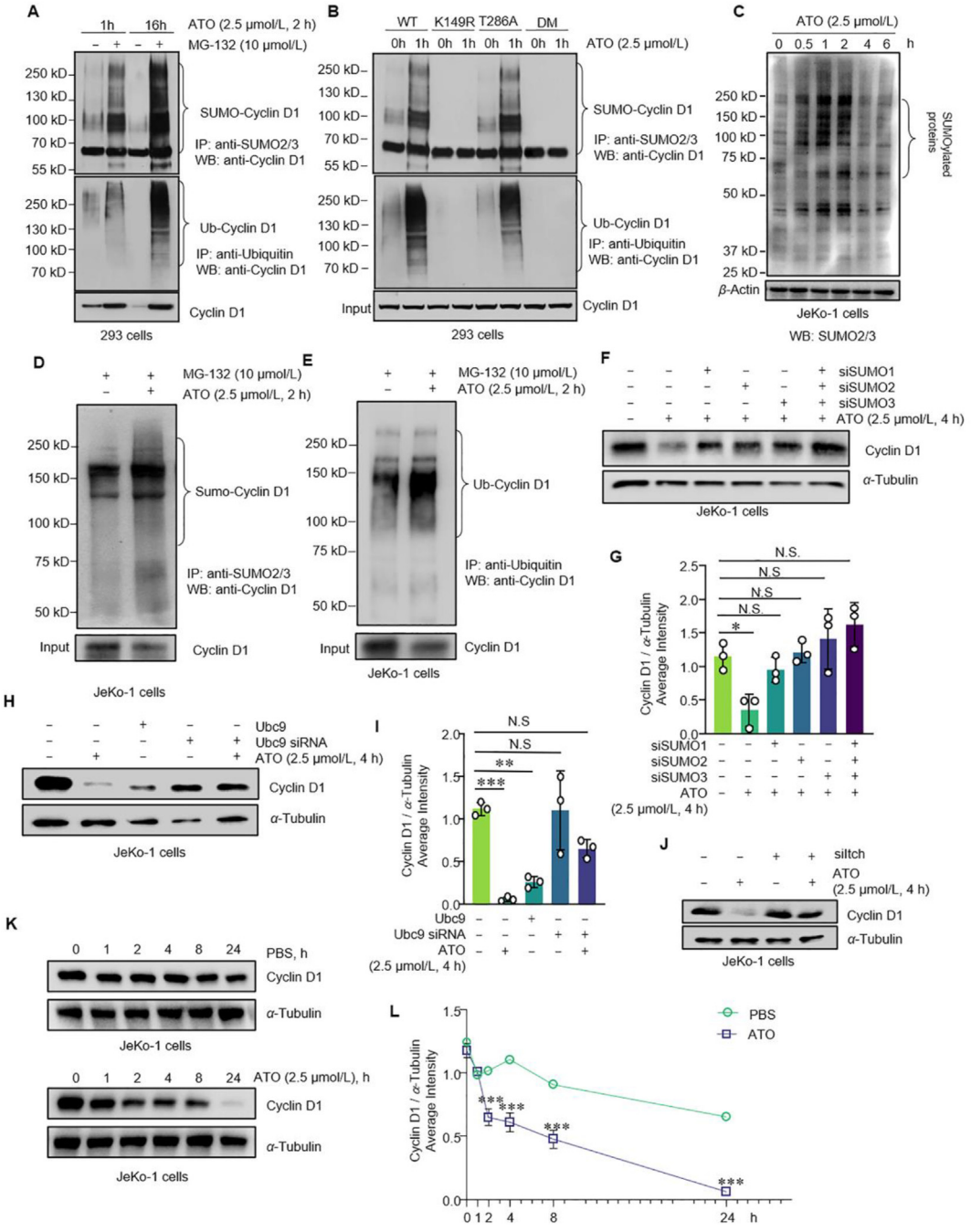

Figure 4 Arsenic trioxide enhances cyclin D1 SUMOylation and degradation. (A) IP assay showing SUMOylation and ubiquitination of cyclin D1 in 293 cells treated with ATO in the absence or presence of MG132. IP was performed using the anti-SUMO2/3 antibody (upper panel) or anti-Ub antibody (lower panel) using the anti-cyclin D1 antibody. Cyclin D1 expression in cell lysates was detected as an input control. (B) IP assay showing SUMOylation and ubiquitination of cyclin D1 in ATO-treated 293 cells transfected with WT or mutant cyclin D1 (K149R, T286A and DM) plasmids. IP was performed using the anti-SUMO2/3 antibody (upper panel) or anti-Ub antibody (lower panel) using the anti-cyclin D1 antibody. Cyclin D1 expression in cell lysates was detected as an input control. (C) SUMO2/3 expression in JeKo-1 cells treated with ATO. (D and E) IP assay showing SUMOylation and ubiquitination of cyclin D1 in JeKo-1 cells treated with ATO in the presence of MG132. IP was performed using the anti-SUMO2/3 antibody (D) or anti-Ub antibody (E) using the anti-cyclin D1 antibody. Cyclin D1 expression in cell lysates was detected as an input control. (F and G) Cyclin D1 expression in JeKo-1 cells transfected with SUMO1/2/3 siRNAs and treated with ATO (F). The Average Intensity of cyclin D1 relative to α-tubulin (G) ($n = 3$). (H and I) Cyclin D1 expression in JeKo-1 cells transfected with Ubc9 plasmid or Ubc9 siRNA and treated with ATO (H). The Average Intensity of cyclin D1 relative to α-tubulin (I) ($n = 3$). (J) Cyclin D1 expression in JeKo-1 cells transfected with Itch siRNA and treated with ATO. (K and L) Cyclin D1 expression in PBS-treated (top) or ATO-treated (bottom) JeKo-1 cells (K). The Average Intensity of cyclin D1 relative to α-tubulin (L). $^*P < 0.05$, $^{**}P < 0.01$, $^{***}P < 0.001$. Data are represented as mean ± SD. Two-way ANOVA followed by Tukey−Kramer test for multiple comparisons (G, I and L).

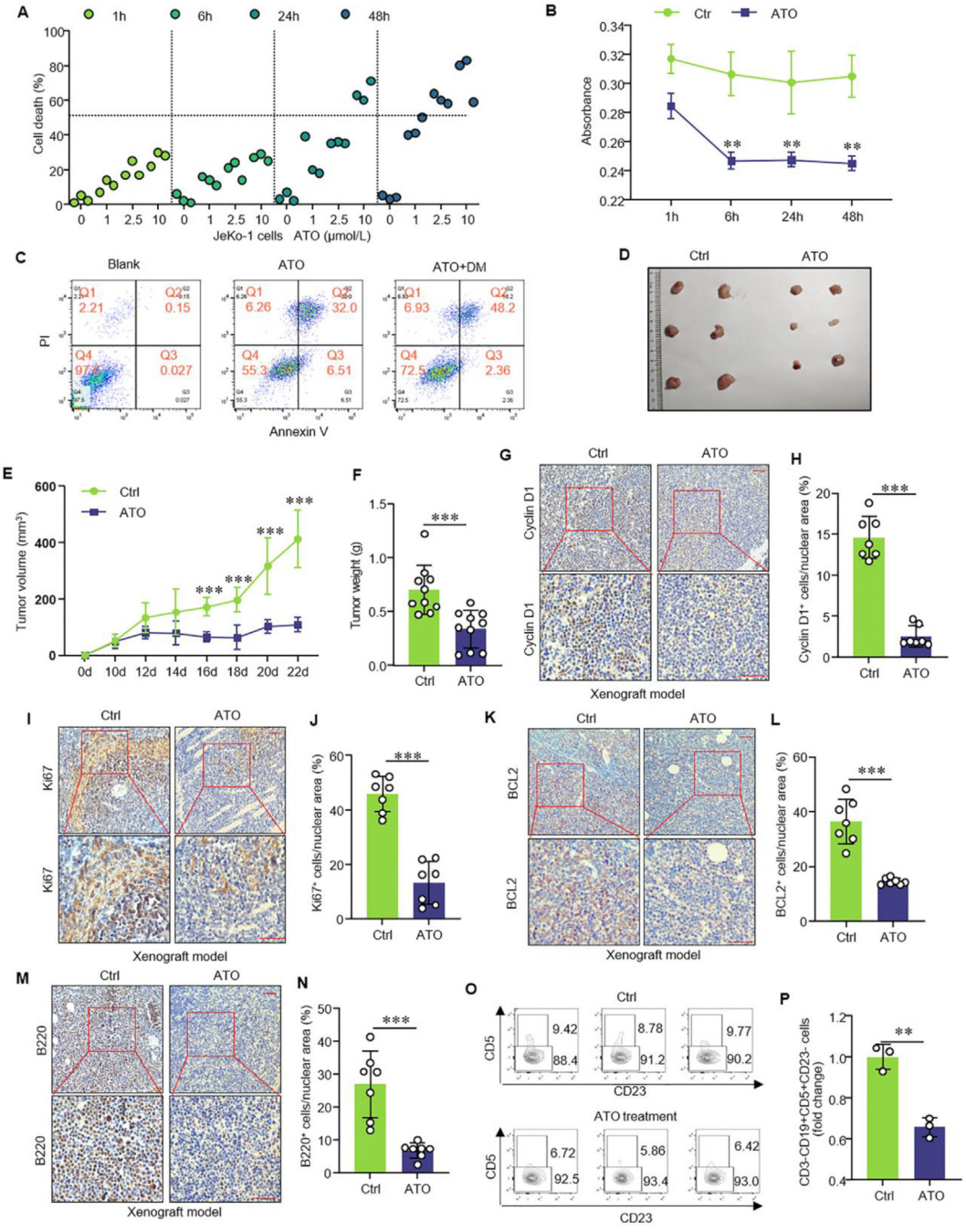

Figure 5 Treatment with arsenic trioxide of SCID mice grafted with MCL cells shows reduced tumor size. (A) Cell death analysis showing the effect of ATO in JeKo-1 cells. JeKo-1 cells were treated with ATO ($n=3$) and the numbers of cell death were counted. (B) CCK8 assay showing cell viability in JeKo-1 cells treated with or without ATO ($n=5$). (C) Flow cytometry assay showing changes in cell apoptosis in JeKo-1 cells transfected with WT or DM cyclin D1 expression plasmid and treated with ATO ($n=3$). Q1: necrotic cells, Q2: apoptotic cells, Q3: pro-apoptotic cells, Q4: live cells. (D) Representative gross anatomy showing tumor size in NCG mice grafted with MCL cells ($n=6$ in each group). (E and F) Quantification of tumor volume (E) and tumor weight (F) of NCG mice grafted with JeKo-1 cells ($n=10$ in each group). (G–N) Representative IHC images showing cell number changes and quantification of cyclin D1+ (G and H), Ki67+ (I and J), Bcl2+ (K and L) and B220+ (M and N) cells in tumor tissues from Ctrl mice or ATO-treated mice (Scale bars, 50 μm) ($n = 7$). (O and P) Flow cytometry images showing numbers and quantification of $CD3^-/CD5^+/CD19^+/CD23^-$ cells in blood in NCG mice grafted with MCL cells with or without ATO treatment ($n = 3$ in each group). $^*P < 0.05$, $^{**}P < 0.01$, $^{***}P < 0.001$. Data are represented as mean ± SD. Two-way ANOVA followed by Tukey–Kramer test for multiple comparisons (B and E), two-tailed unpaired Student's *t*-test analysis (F and P).

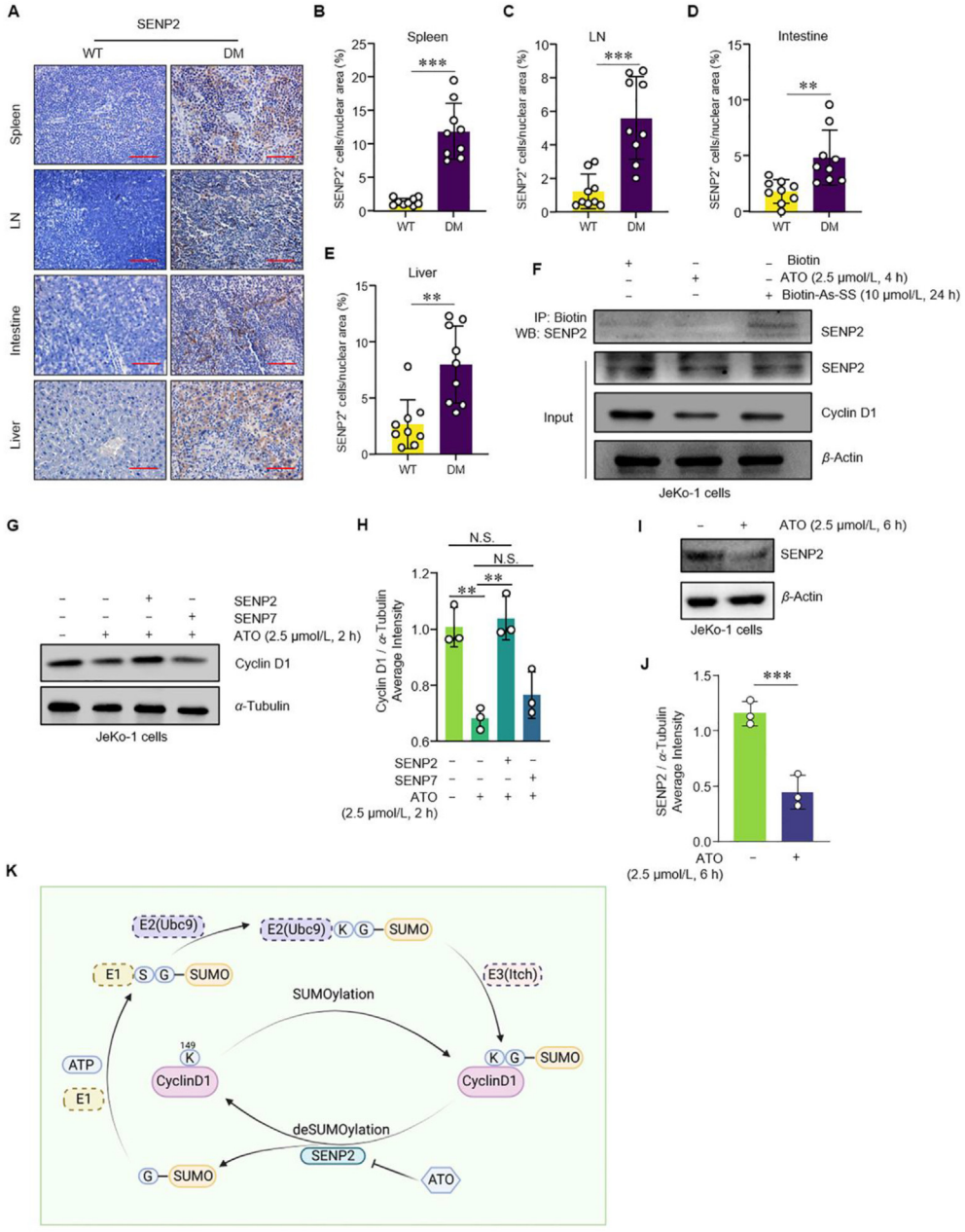

Figure 6 Arsenic trioxide inhibits SENP2 expression in DM mice. (A−E) Representative immunohistochemistry (IHC) images showing changes in SENP2$^+$ cells in spleen, lymph node (LN), intestine and liver tissues derived from WT and DM mice ($n=9$) (Scale bars, 50 μm). (F) IP assay showing ATO interaction with SENP2 in JeKo-1 cells treated with Biotin, ATO or Biotin-As-SS. IP was performed using the anti-Biotin antibody followed by the Western blot using the anti-SENP2 antibody. SENP2 expression in cell lysates was detected as an input control. Cyclin D1 expression was also detected in JeKo-1 cells. (G and H) Representative WB showing cyclin D1 expression in JeKo-1 cells transfected with SENP2 or SENP7 plasmid and treated with ATO. The average intensity of cyclin D1 relative to α-tubulin (H). (I and J) Representative WB showing SENP2 expression in JeKo-1 cells treated with or without ATO. The Average Intensity of SENP2 relative to α-tubulin (J). (K) A schematic diagram illustrating the mechanism by which ATO promotes cyclin D1 degradation. $*P < 0.05$, $**P < 0.01$, $***P < 0.001$. Data are represented as mean ± SD. Two-tailed unpaired Student's *t*-test analysis (B−E).

expression, thus ATO inhibit the expression of SENP2 leading to enhance cyclin D1 degradation (Fig. 6K).

4. Discussion

Cyclin D1 has been known as an oncogene because it is upregulated in many different types of cancers, including breast cancer, MCL, urinary bladder cancer, and prostate cancer[1,41]. However, which type of cancer is truly cyclin D1-dependent is currently unknown. It has been shown that forced expression of cyclin D1 in mammary tissues causes development of breast cancer in mice[42-44]. The role of cyclin D1 was further demonstrated by the fact that breast cancer development is delayed when *cyclin D1* is deleted in a Neu virus-induced breast cancer animal model[45,46]. These findings suggest that cyclin

D1 plays an important role in breast cancer development. However, if breast cancer is more sensitive to cellular cyclin D1 levels still unknown. In this study, we blocked cyclin D1 degradation by mutations of both phosphorylation and SUMOylation sites of cyclin D1. Only a MCL phenotype was observed in cyclin D1 DM mice, suggesting that cyclin D1 plays a unique role in a subpopulation of B lymphocytes, although how cyclin D1 causes cell transformation in these cells is still unknown.

Since phosphorylation mutant cyclin D1 could be degraded by the ubiquin−proteasome system, this finding suggests that the mechanism other than phosphorylation-mediated ubiquitin−proteasome degradation is involved in the cyclin D1 degradation. In this study, we determined if cyclin D1 is SUMOylated, and we found that cyclin D1 is indeed SUMOylated and that SUMOylation of cyclin D1 leads to its ubiquitination and proteasome degradation. We also identified Itch as a specific E3 ligase that recognizes SUMOylated cyclin D1, and we mapped the SUMO-interacting motifs in the Itch protein. Our *in vitro* data suggest that SUMOylation-dependent degradation of cyclin D1 acts independently from phosphorylation-induced degradation, but that both pathways are needed to fully regulate this process. And our *in vivo* data further support this notion as we found that only cyclin D1 DM mice exhibit a MCL phenotype, although K149R cyclin D1 mutant mice had a weak neoplastic phenotype in the lymph system. Although we found that cyclin D1 protein degradation is mediated by phosphorylation- and SUMOylation-mediated ubiquitin−proteasome mechanisms and T286 and K149 are the critical phosphorylation and SUMOylation sites for cyclin D1 degradation, up to date, only T286 mutation has been found in the human cancer[47] and K149 mutation has not been identified in human cancers. Further studies with deep screening for the cancer mutations need to be conducted to determine if K149 mutations can be found in cancer cells, especially blood cancers, such as Mantle cell lymphoma.

Arsenic trioxide (ATO) has been shown to be a powerful agent to induce PML protein SUMOylation[30-32] and is an effective drug to treat acute promyelocytic leukemia (APL)[39,48], for which it received approval by the US Food and Drug Administration in 2000. In this study, we demonstrated that ATO enhanced cyclin D1 SUMOylation and subsequent ubiquitination and proteasome degradation. We further demonstrated that ATO specifically bound to and inhibited the deSUMOylation enzyme, SENP2, leading to the enhancement of cyclin D1 SUMOylation and proteasome degradation. Although our initial data pointed to that ATO may bind and inhibit SENP2 in MCL cells leading to the enhancement of cyclin D1 SUMOylation, large amount additional works need to be done to definitely prove that ATO is indeed involved in the enhancement of cyclin D1 SUMOylation.

We further confirmed the positive role of ATO in inhibiting tumor growth in SCID mice grafted with MCL cells. These findings suggest that ATO may be an option for MCL treatment. It has been reported that an oral ATO-based regimen is effective for the treatment of relapsed/refractory MCL in a small pilot study[49], which was initiated based on a prior *in vitro* study showing positive effects of the drug on lymphoma[50]. However, the molecular mechanism by which ATO might improve outcome in MCL was not established. Here, we provide new evidence that ATO enhances cyclin D1 SUMOylation by inhibiting the SENP2 expression. These findings provide an opportunity to develop novel drugs to treat MCL, AML and other related cancers, including ASO but also others that target the SUMOylation pathway.

Although ATO has been shown to enhance PML protein SUMOylation[30-32] in APL cells, the detail mechanism of action of ATO in PML SUMOylation remains unknown, based on our findings, we speculate that ATO may enhance PML SUMOylation by inhibiting PML deSUMOylation in APL cells. This hypothesis needs to be further verified.

ATO has been shown to enhance PML protein SUMOylation and is an effective drug to treat APL[30-32]. Since cyclin D1 is also upregulated in other leukemia cells, such as human acute lymphoblastic leukemia (ALL)[51], it is conceivable that ATO may treat APL effectively by enhancing SUMOylation of both PML and cyclin D1 proteins in APL cells. The effect and mechanism of ATO on cyclin D1 SUMOylation in APL cells need to be further investigated.

In this study we demonstrated that accumulation of cyclin D1 in a specific subpopulation of lymphocytes leads to MCL and ATO could treat MCL by inhibiting cyclin D1 deSUMOylation. Since cyclin D1 upregulation has been found in many different types of cancers, our findings suggest that agents affecting cyclin D1 deSUMOylation may be used for the treatment of multiple types of cancers.

In summary, we demonstrated that cyclin D1 is SUMOylated and SUMOylation of cyclin D1 leads to its ubiquitination and proteasome degradation. We identified a specific E3 ligase, Itch, that recognizes SUMOylated cyclin D1 and mapped the SUMO-interacting motifs in the Itch protein. We found that SUMOylation-mediated cyclin D1 degradation is independent from phosphorylation-mediated cyclin D1 degradation. We then generated three strains of cyclin D1 mutant mice with mutations in the cyclin D1 SUMOylation site, phosphorylation site or both sites. We characterized the three cyclin D1 mutant mice and found an MCL-like phenotype in the cyclin D1 DM mice, suggesting that sufficient accumulation of endogenous cyclin D1 to induce B cell lymphoma requires inhibition of both SUMOylation- and phosphorylation-mediated proteasome degradation of cyclin D1. We also found that ATO enhances cyclin D1 SUMOylation, and thus its degradation, through inhibition of cyclin D1 deSUMOylation enzyme-SENP2. Such alterations in the SUMOylation of cyclin D1 by ATO was sufficient to inhibit tumor growth in SCID mice grafted with MCL cells.

Acknowledgments

We would like to express our gratitude to Drs. Jian Huang and Lan Zhao for helping us generate and maintain the cyclin D1 mutant mice. This work was supported by National Key Research and Development Program of China (2021YFB3800800) to Di Chen and Liping Tong. This project has also been supported by the National Natural Science Foundation of China (NSFC) grants (82030067, 82161160342 and 82250710174) to Di Chen and grant (82302757) to Ke Lu. Ke Lu was also supported by SIAT Innovation Program for Excellent Young Researchers.

Author contributions

Di Chen conceived and designed the work; Ke Lu, Ming Zhang, Siyu Shen, Haiqing Song and Hongyu Qin obtained the data; Ke Lu, Siyu Shen, Hongyu Qin, and Hua Jiang analyzed the data; Di Chen provided funding support; Di Chen and Ke Lu drafted the manuscript; Guozhi Xiao, Liping Tong, Qing Jiang, and Di Chen revised the manuscript.

Conflicts of interest

The authors declare that the research was conducted in the absence of any commercial or financial relationships that could be construed as a potential conflict of interest.

Appendix A. Supporting information

Supporting information to this article can be found online at https://doi.org/10.1016/j.apsb.2024.03.013.

References

1. Qie S, Diehl JA. Cyclin D1, cancer progression, and opportunities in cancer treatment. *J Mol Med (Berl)* 2016;**94**:1313−26.
2. Alao JP. The regulation of cyclin D1 degradation: roles in cancer development and the potential for therapeutic invention. *Mol Cancer* 2007;**6**:24.
3. Klein EA, Assoian RK. Transcriptional regulation of the cyclin D1 gene at a glance. *J Cell Sci* 2008;**121**:3853−7.
4. Diehl JA, Zindy F, Sherr CJ. Inhibition of cyclin D1 phosphorylation on threonine-286 prevents its rapid degradation *via* the ubiquitin−proteasome pathway. *Genes Dev* 1997;**11**:957−72.
5. Guo Y, Yang K, Harwalkar J, Nye JM, Mason DR, Garrett MD, et al. Phosphorylation of cyclin D1 at Thr 286 during S phase leads to its proteasomal degradation and allows efficient DNA synthesis. *Oncogene* 2005;**24**:2599−612.
6. Bartkova J, Lukas J, Muller H, Lutzhoft D, Strauss M, Bartek J. Cyclin D1 protein expression and function in human breast cancer. *Int J Cancer* 1994;**57**:353−61.
7. Zukerberg LR, Yang WI, Gadd M, Thor AD, Koerner FC, Schmidt EV, et al. Cyclin D1 (PRAD1) protein expression in breast cancer: approximately one-third of infiltrating mammary carcinomas show overexpression of the cyclin D1 oncogene. *Mod Pathol* 1995;**8**:560−7.
8. Bosch F, Jares P, Campo E, Lopez-Guillermo A, Piris MA, Villamor N, et al. PRAD-1/cyclin D1 gene overexpression in chronic lymphoproliferative disorders: a highly specific marker of mantle cell lymphoma. *Blood* 1994;**84**:2726−32.
9. Wagner U, Suess K, Luginbuhl T, Schmid U, Ackermann D, Zellweger T, et al. Cyclin D1 overexpression lacks prognostic significance in superficial urinary bladder cancer. *J Pathol* 1999;**188**:44−50.
10. Drobnjak M, Osman I, Scher HI, Fazzari M, Cordon-Cardo C. Overexpression of cyclin D1 is associated with metastatic prostate cancer to bone. *Clin Cancer Res* 2000;**6**:1891−5.
11. Gautschi O, Ratschiller D, Gugger M, Betticher DC, Heighway J. Cyclin D1 in non-small cell lung cancer: a key driver of malignant transformation. *Lung Cancer* 2007;**55**:1−14.
12. Ogino S, Nosho K, Irahara N, Kure S, Shima K, Baba Y, et al. A cohort study of cyclin D1 expression and prognosis in 602 colon cancer cases. *Clin Cancer Res* 2009;**15**:4431−8.
13. Musgrove EA, Caldon CE, Barraclough J, Stone A, Sutherland RL. Cyclin D as a therapeutic target in cancer. *Nat Rev Cancer* 2011;**11**:558−72.
14. Germain D, Russell A, Thompson A, Hendley J. Ubiquitination of free cyclin D1 is independent of phosphorylation on threonine 286. *J Biol Chem* 2000;**275**:12074−9.
15. Sternsdorf T, Jensen K, Reich B, Will H. The nuclear dot protein sp100, characterization of domains necessary for dimerization, subcellular localization, and modification by small ubiquitin-like modifiers. *J Biol Chem* 1999;**274**:12555−66.
16. Le Drean Y, Mincheneau N, Le Goff P, Michel D. Potentiation of glucocorticoid receptor transcriptional activity by sumoylation. *Endocrinology* 2002;**143**:3482−9.
17. Bae SH, Jeong JW, Park JA, Kim SH, Bae MK, Choi SJ, et al. Sumoylation increases HIF-1alpha stability and its transcriptional activity. *Biochem Biophys Res Commun* 2004;**324**:394−400.
18. Jackson SP, Durocher D. Regulation of DNA damage responses by ubiquitin and SUMO. *Mol Cell* 2013;**49**:795−807.
19. Di Bacco A, Ouyang J, Lee HY, Catic A, Ploegh H, Gill G. The SUMO-specific protease SENP5 is required for cell division. *Mol Cell Biol* 2006;**26**:4489−98.
20. Flotho A, Melchior F. Sumoylation: a regulatory protein modification in health and disease. *Annu Rev Biochem* 2013;**82**:357−85.
21. Seufert W, Futcher B, Jentsch S. Role of a ubiquitin-conjugating enzyme in degradation of S- and M-phase cyclins. *Nature* 1995;**373**:78−81.
22. Seeler JS, Dejean A. SUMO and the robustness of cancer. *Nat Rev Cancer* 2017;**17**:184−97.
23. Jentsch S, Psakhye I. Control of nuclear activities by substrate-selective and protein-group SUMOylation. *Annu Rev Genet* 2013;**47**:167−86.
24. Schick M, Zhang L, Maurer S, Maurer HC, Isaakaidis K, Schneider L, et al. Genetic alterations of the SUMO isopeptidase SENP6 drive lymphomagenesis and genetic instability in diffuse large B-cell lymphoma. *Nat Commun* 2022;**13**:281.
25. Samikkannu T, Chen CH, Yih LH, Wang AS, Lin SY, Chen TC, et al. Reactive oxygen species are involved in arsenic trioxide inhibition of pyruvate dehydrogenase activity. *Chem Res Toxicol* 2003;**16**:409−14.
26. Aposhian HV, Aposhian MM. Arsenic toxicology: five questions. *Chem Res Toxicol* 2006;**19**:1−15.
27. Park WH, Seol JG, Kim ES, Hyun JM, Jung CW, Lee CC, et al. Arsenic trioxide-mediated growth inhibition in MC/CAR myeloma cells *via* cell cycle arrest in association with induction of cyclin-dependent kinase inhibitor, p21, and apoptosis. *Cancer Res* 2000;**60**:3065−71.
28. Miller Jr WH, Schipper HM, Lee JS, Singer J, Waxman S. Mechanisms of action of arsenic trioxide. *Cancer Res* 2002;**62**:3893−903.
29. Lo RK, Kwong YL. Arsenic trioxide suppressed mantle cell lymphoma by downregulation of cyclin D1. *Ann Hematol* 2014;**93**:255−65.
30. Tatham MH, Geoffroy MC, Shen L, Plechanovova A, Hattersley N, Jaffray EG, et al. RNF4 is a poly-SUMO-specific E3 ubiquitin ligase required for arsenic-induced PML degradation. *Nat Cell Biol* 2008;**10**:538−46.
31. Zhang XW, Yan XJ, Zhou ZR, Yang FF, Wu ZY, Sun HB, et al. Arsenic trioxide controls the fate of the PML-RARalpha oncoprotein by directly binding PML. *Science* 2010;**328**:240−3.
32. Lallemand-Breitenbach V, Jeanne M, Benhenda S, Nasr R, Lei M, Peres L, et al. Arsenic degrades PML or PML-RARalpha through a SUMO-triggered RNF4/ubiquitin-mediated pathway. *Nat Cell Biol* 2008;**10**:547−55.
33. Heredia-Moya J, Kirk KL. An improved synthesis of arsenic−biotin conjugates. *Bioorg Med Chem* 2008;**16**:5743−6.
34. Newman RM, Mobascher A, Mangold U, Koike C, Diah S, Schmidt M, et al. Antizyme targets cyclin D1 for degradation. A novel mechanism for cell growth repression. *J Biol Chem* 2004;**279**:41504−11.
35. Magnifico A, Ettenberg S, Yang C, Mariano J, Tiwari S, Fang S, et al. WW domain HECT E3s target Cbl RING finger E3s for proteasomal degradation. *J Biol Chem* 2003;**278**:43169−77.
36. Santra MK, Wajapeyee N, Green MR. F-box protein FBXO31 mediates cyclin D1 degradation to induce G1 arrest after DNA damage. *Nature* 2009;**459**:722−5.
37. Kuo PY, Jatiani SS, Rahman AH, Edwards D, Jiang Z, Ahr K, et al. SOX11 augments BCR signaling to drive MCL-like tumor development. *Blood* 2018;**131**:2247−55.
38. Huang C, Yin Q, Meng J, Zhu W, Yang Y, Qian X, et al. Versatile probes for the selective detection of vicinal-dithiol-containing proteins: design, synthesis, and application in living cells. *Chemistry* 2013;**19**:7739−47.
39. Huang XJ, Wiernik PH, Klein RS, Gallagher RE. Arsenic trioxide induces apoptosis of myeloid leukemia cells by activation of caspases. *Med Oncol* 1999;**16**:58−64.
40. Reverter D, Lima CD. Structural basis for SENP2 protease interactions with SUMO precursors and conjugated substrates. *Nat Struct Mol Biol* 2006;**13**:1060−8.
41. Jares P, Colomer D, Campo E. Molecular pathogenesis of mantle cell lymphoma. *J Clin Invest* 2012;**122**:3416−23.

42. Wang TC, Cardiff RD, Zukerberg L, Lees E, Arnold A, Schmidt EV. Mammary hyperplasia and carcinoma in MMTV-cyclin D1 transgenic mice. *Nature* 1994;**369**:669−71.
43. Landis MW, Pawlyk BS, Li T, Sicinski P, Hinds PW. Cyclin D1-dependent kinase activity in murine development and mammary tumorigenesis. *Cancer Cell* 2006;**9**:13−22.
44. Spring LM, Wander SA, Andre F, Moy B, Turner NC, Bardia A. Cyclin-dependent kinase 4 and 6 inhibitors for hormone receptor-positive breast cancer: past, present, and future. *Lancet* 2020;**395**:817−27.
45. Lee RJ, Albanese C, Fu M, D'Amico M, Lin B, Watanabe G, et al. Cyclin D1 is required for transformation by activated Neu and is induced through an E2F-dependent signaling pathway. *Mol Cell Biol* 2000;**20**:672−83.
46. Yu Q, Geng Y, Sicinski P. Specific protection against breast cancers by cyclin D1 ablation. *Nature* 2001;**411**:1017−21.
47. Goshima T, Habara M, Maeda K, Hanaki S, Kato Y, Shimada M. Calcineurin regulates cyclin D1 stability through dephosphorylation at T286. *Sci Rep-Uk* 2019;**9**:12779.
48. de Thé H. Differentiation therapy revisited. *Nat Rev Cancer* 2018;**18**: 117−27.
49. Gill H, Au WY, Cheung WW, Lee EY, Kwong YL. Oral arsenic trioxide-based regimen as salvage treatment for relapsed or refractory mantle cell lymphoma. *Ann Oncol* 2014;**25**:1391−7.
50. Zhu XH, Shen YL, Jing YK, Cai X, Jia PM, Huang Y, et al. Apoptosis and growth inhibition in malignant lymphocytes after treatment with arsenic trioxide at clinically achievable concentrations. *J Natl Cancer Inst* 1999;**91**:772−8.
51. Jaroslav P, Martina H, Jiri S, Hana K, Petr S, Tomas K, et al. Expression of cyclins D1, D2, and D3 and Ki-67 in leukemia. *Leuk Lymphoma* 2005;**46**:1605−12.